Received: 3 December 2024 | Revised: 19 March 2025 | Accepted: 25 March 2025

DOI: 10.1096/fj.202403086RR

RESEARCH ARTICLE

The FASEB Journal

Proteomic analysis of liver fibrosis reveals EFEMP1 as a new modulator of focal adhesion and migration of hepatic stellate cells

Célia Thomas | **Fidaa Bouezzedine** | **Dominique Bonnier** | **Vincent Legagneux** | **Nathalie Théret**

Univ Rennes, INSERM, EHESP, Institut de Recherche en Santé, Environnement et Travail (IRSET), UMR_S 1085, Rennes, France

Correspondence
Nathalie Théret, Univ Rennes, INSERM, EHESP, Institut de Recherche en Santé, Environnement et Travail (IRSET), UMR_S 1085, 2 Avenue Pr. Léon. Bernard, Rennes 35043, France.
Email: nathalie.theret@inserm.fr

Funding information
Institut National de la Santé et de la Recherche Médicale (INSERM); Université de Rennes; la Ligue Nationale Contre le Cancer; Région Bretagne

Abstract

Liver fibrosis is characterized by an excessive accumulation of extracellular matrix (ECM) leading to liver dysfunction. Proteomic approaches help to decipher ECM alterations during fibrosis progression. Using a decellularization method, we performed a proteomic analysis of 18 fibrotic human liver samples and identified 106 deregulated ECM proteins. Three members of the fibulin protein family (fibulin-2, -3, and -5) expressed by hepatic stellate cells were significantly associated with fibrosis progression. Integrative analyses of protein–protein interaction networks highlighted different functional annotations for these three fibulins. Gene silencing studies showed that unlike fibulin-2 (*FBLN2*), fibulin-3 (*EFEMP1*) depletion impaired focal adhesions, FAK phosphorylation, the fibronectin network, and cell migration. These findings are the first to demonstrate the critical involvement of fibulin-3 in the regulation of hepatic stellate cell focal adhesions and migration, emphasizing the intricate link between chronic liver disease progression and remodeling of the microenvironment.

KEYWORDS

EFEMP1, fibulin, focal adhesion, hepatic stellate cell, liver fibrosis, migration, proteomics

Abbreviations: ANXA5, annexin A5; cDC2, conventional dendritic cell; Col18A1, collagen type XVIII alpha 1 chain; Col4A1, collagen type IV alpha 1 chain; Col5A3, collagen type V alpha 3 chain; CTSB, cathepsin B; ECM, extracellular matrix; EFEMP1/FBLN3, EGF containing fibulin extracellular matrix protein 1/fibulin-3; ELN, elastin; EMILIN, elastin microfibril interfacer 1; ERdj5, DnaJ heat shock protein family (Hsp40) member C10; FAK, focal adhesion kinase; FBLN2, fibulin-2; FBLN5, fibulin-5; FBN1, fibrillin-1; FBN2, fibrillin-2; FN1, fibronectin; GO, gene ontology; HBV, hepatitis B virus; HCC, hepatocellular carcinoma; HCV, hepatitis C virus; HSC, hepatic stellate cell; INHBE, inhibin subunit beta E; ITGA5, integrin α5; LAMA4, laminin subunit alpha 4; LTBP4, latent transforming growth factor beta binding protein 4; MFAP1, MFAP2, MFAP3, MFAP4, MFAP5, microfibril-associated protein 1, 2, 3, 4, 5; MMP9, matrix metalloproteinase-9; NAFLD, non-alcoholic fatty acid liver disease; NK, natural killer cell; NKT, natural killer T cell; P4HB, prolyl 4-hydroxylase subunit beta; PAI-1, plasminogen activator inhibitor-1; PAX, paxillin; PDIA4, protein disulfide isomerase family A member 4; PDIA6, protein disulfide isomerase family A member 6; PPI, protein–protein interaction; RCN1, reticulocalbin 1; RPE, reticulum pigment epithelium; SDF2L1, stromal cell-derived factor 2 Like 1; TGF-β, tumor growth factor beta; TXNDC5, thioredoxin domain containing 5; VTN, vitronectin; VWF, Von Willebrand factor.

1 | INTRODUCTION

Most chronic liver diseases are associated with the development of fibrosis, of which cirrhosis is the end-stage and the main risk factor for hepatocellular carcinoma. Liver diseases, mainly caused by viral hepatitis B or C (HBV, HCV), alcohol consumption, and non-alcoholic fatty liver (NAFLD), and cirrhosis are recognized as a major cause of morbidity worldwide.[1,2] Understanding and characterizing the fibrotic microenvironment has the potential to enable the identification of novel biomarkers and therapeutic targets, or methods to facilitate drug delivery.

Fibrosis is characterized by an excessive accumulation of extracellular matrix (ECM), resulting in liver dysfunction. Hepatic stellate cells play a critical role in liver fibrosis as a main source of ECM and remodeling activity. The ECM is defined as a complex molecular network comprising collagen, glycoproteins, and proteoglycans, all of which constitute the core of the matrisome that is complemented by ECM-associated proteins such as matrix remodeling regulators and growth factors.[3,4] The ECM is a dynamic structure with various compositions and mechanical properties, constituting a wide variety of cellular microenvironments that evolve over the course of the development of liver fibrosis and with its etiologies. In recent years, proteomic approaches have been used to characterize ECM alterations in chronic liver lesions. Analyses of fibrotic tissues from patients with viral hepatitis C have shown global alterations in the parenchymal proteome[5,6] while the microdissection of cirrhotic areas identified 24 proteins whose amounts are altered in fibrosis tissues, including the cirrhosis-associated human microfibril–associated protein 4 (MFAP-4).[7]

Using a label-free discovery approach, Bracht et al.[8] identified 60 proteins differentially up-regulated in a high fibrosis group of patients with HBV and HCV viral hepatitis. More recently, decellularization methods used to purify ECM scaffolds from fibrotic tissues have identified protein signatures corresponding to various stages of HCV-related liver fibrosis, based on the differential detection of 47 proteins.[6] Similarly, Mazza et al.[9] identified 51 proteins significantly enriched in cirrhotic ECM scaffolds (compared to healthy ECM) prepared from human liver tissues, and Daneshgar et al.[10] identified 59 differentially expressed proteins in various fibrotic ECM scaffolds. Decellularization and ECM-enriched protocols have also been successfully applied to tissue samples from fibrosis-induced mouse models to characterize ECM changes following acute and chronic injuries.[11–13] Although informative, the number of such studies remains limited, especially in human tissues and for nonviral etiologies. Therefore, there is a critical need to further investigate and characterize proteomic changes associated with liver fibrosis. Here we performed a proteomic analysis of 18 human fibrotic liver samples using the decellularization procedure described by Naba et al.[14] to extract ECM-enriched proteins. Among the deregulated proteins, we showed that the amounts of three members of the fibulin protein family (fibulin-2, -3. and -5) were associated with fibrosis progression. Furthermore, an analysis of protein–protein interaction networks revealed different functional annotations for these three fibulins. Using a hepatic stellate cell line, we showed that gene silencing of *EFEMP1* (fibulin-3) but not *FBLN2* (fibulin-2) impaired focal adhesions, FAK phosphorylation, and cell migration. Our data demonstrate the specific function of fibulin-3 in modulating hepatic stellate cell adhesion and migration.

2 | MATERIALS AND METHODS

2.1 | Human samples

Fifty non-tumor liver samples were taken from patients who had undergone hepatectomy for hepatocellular carcinoma (HCC), 18 of which were selected for the proteomic analysis (Table S1). Histological stages of fibrosis were graded according to the METAVIR score: F1, portal fibrosis without septa; F2, portal fibrosis with rare septa; F3, numerous septa without cirrhosis; and F4, cirrhosis. All tissue sections were routinely analyzed after staining with hematoxylin–eosin–saffron and Sirius red. Liver samples were from the Biological Resources Center (BRC) at Rennes University Hospital. Access to this material was in agreement with French laws and satisfied the requirements of the local Ethics Committee.

2.2 | Proteomic analyses of ECM from human fibrotic tissue samples

Tissue preparation and ECM protein enrichment were performed as previously described.[15] Briefly, tissue samples (stages F1–F4) were mechanically homogenized and extracted sequentially using Naba's protocol.[14] Protein digestion and mass spectrometry analyses were performed by the Proteomics Platform of the CHU de Québec Research Center (Quebec, Qc, Canada) using LC–MS/MS on Orbitrap Fusion (Thermo Fisher Scientific). Mass spectra were interpreted with MaxQuant/Andromeda and MS/MS spectra were searched against the UniprotKB Homo sapiens (CP_Homo-Sapiens) database with fixed modification: carbamidomethyl(C), variable modifications: oxidation (M), oxidation (K), oxidation (P). Peptide identifications were filtered at a 1% false discovery rate. Resulting label-free quantitation (LFQ) values were

compared between normal liver samples (F0) and samples corresponding to each fibrosis stage (F1, F2, F3, and F4), using a nonparametric test (Mann–Whitney). Comparisons were performed from either raw values, rank values, or values normalized to the median value in each sample. Proteins were judged to be differentially expressed when their amounts were found to be significantly increased or decreased between at least two groups of samples, with at least one of these normalization methods.

2.3 | Protein–protein interaction networks

Gene symbols for each fibulin were used to query molecular interaction databases using the Proteomics Standard Initiative Common QUery InterfaCe (PSICQUIC).[16] This specification was created by the Human Proteome Organization Proteomics Standards Initiative (HUPO-PSI) to standardize access to molecular interaction databases. In this study, queries were performed on February 22, 2024.

2.4 | Cell culture and transfection

Primary human hepatocytes (HH) and hepatic stellate cells (HSCs) were obtained after isolation from histologically normal regions of partial hepatectomies from patients undergoing hepatic resection for liver metastases from colorectal cancers as previously described.[17] HH and HSCs were cultured in Dulbecco's minimal essential medium (DMEM) containing 4.5 g/L glucose, pyruvate, glutamine, penicillin (100 IU/mL), streptomycin (100 mg/mL), and supplemented with 10% fetal bovine serum (FBS; Lonza). The LX-2 cell line was maintained in DMEM with 4.5 g/L glucose, pyruvate, glutamine, penicillin (100 IU/mL), streptomycin (100 mg/mL), and 10% FBS (Eurobio). When indicated, cells were treated with IL-1β (3 ng/mL) or TGF-β (5 ng/mL) for the indicated durations in media containing 2% FBS. LX2 cells were transfected with pCMV5-Flag-EFEMP1 from the laboratory of J. Hullemann, using Lipofectamine 2000 (Invitrogen; Thermo Fisher) according to the manufacturer's instructions.

2.5 | Immunofluorescence

For F-actin staining, LX-2 cells were seeded in 12-well plates either coated with collagen I or uncoated (plastic surface) 24 h after siRNA transfection and cultured for an additional 72 h. Transfected cells were fixed for 10 min in 4% paraformaldehyde, followed by permeabilization with 0.1% Triton X-100 in PBS for 10 min and were washed three times in PBS. F-actin was stained using phalloidin coupled with Alexa-488 (1/40; #8878, Cell Signaling). Fixed cells were counterstained with Hoechst-33342 and observed under epifluorescence microscopy. Images were obtained using a Zeiss Axio Vert A1 microscope and were analyzed with ImageJ/FiJi software. For nuclear size analysis, regions of interest (ROIs) corresponding to the projected areas of nuclei (Hoechst signal) were defined by automatic thresholding. For each ROI and channel, area, average signal value, and integrated signal value were collected. Analyses of measurement tables were performed in R.

For other immunostainings, LX-2 cells were seeded in μ-slide eight-well IbiTreat (#80806, Ibidi) 24 h after siRNA transfection and cultured for an additional 72 h. Transfected cells were fixed for 10 min in 4% paraformaldehyde and washed three times in PBS. For paxillin detection, cells were permeabilized with 0.1% Triton X-100 in PBS for 10 min. Fixed cells were incubated for 2 h at room temperature in PBS containing 1% BSA followed by overnight incubation at 4°C with primary antibodies: anti-paxillin (1/100; mouse; #612405, BD Transduction Laboratories), anti-fibronectin (1/40; rabbit; #PA5-29578, Invitrogen) or anti-integrin α5 (1/25; mouse; #MABT201; Sigma-Aldrich) diluted in PBS-1% BSA. Bound antibodies were detected with a secondary Cy3-conjugated donkey anti-mouse IgG antibody (1/100; #715-165-150, Jackson Immunoresearch) or donkey anti-rabbit IgG antibody (1/100, #711-165-152, Jackson Immunoresearch). Images were obtained using a TCS SP8 confocal microscope (Leica) with the Leica Application Suite Advanced Fluorescence and analyzed with ImageJ/FiJi software. Quantification of the number and size of fibronectin length was done as previously described.[18] For integrin α5 analysis, ROIs corresponding to positively labeled objects were defined in all focal planes by automatic threshold. Particles with a minimal size of 3 μm^2 were analyzed with shape descriptors, and the roundness of integrin α5 particles was measured. An average roundness was calculated for each picture. After discarding overlapping fields, a minimum of five independent pictures were used for comparisons between conditions in three independent experiments.

2.6 | Focal adhesion analysis

Focal adhesions were detected based on paxillin immunostaining and imaged with a SP8 confocal microscope (Leica). Image analyses were performed with ImageJ/Fiji software. Optical slices containing paxillin signals were Z-projected and summed, then thresholded using

the Otsu algorithm. Paxillin foci larger than 1 μm^2 were counted and normalized to the number of nuclei (objects larger than 100 μm^2 in the DAPI channel).

2.7 | Gene silencing by RNA-interference

siRNA transfections were performed with Lipofectamine® RNAiMAX Reagent (Invitrogen) according to the manufacturer's instructions. LX-2 cells were transfected with *EFEMP1*, *FBLN2*, or control siRNAs for the indicated times. The following siRNAs (Eurogentec) sequences were used:

siEFEMP1 si1 (sense): GUGUGUCAACCACUAUGGAdTdT
siEFEMP1 si2 (sense): GGAAACACAACCAGCAGAAdTdT
siEFEMP1 si3 (sense): GACAUUGAUGAAUGCAGAAdTdT
siFBLN2 (sense): GAGUUUCAGAGGCAGAGAUdTdT
siCTRL (negative control): Eurogentec reference SR-CL000-005.

After validation, siEFEMP1 si2 was selected for *EFEMP1* knockdown experiments.

2.8 | RNA isolation and real-time quantitative PCR

Total RNA of liver samples and cultured cells was extracted using the TRIzol reagent (Invitrogen) according to the manufacturer's instructions. cDNAs were obtained by reverse transcription from 1 µg of total RNA using the high-capacity cDNA reverse transcription kit (Applied Biosystems) and quantified by real-time quantitative PCR using the Power-SYBR-Green PCR Master Mix (Applied Biosystems). Transcript abundance was normalized using the GAPDH reference gene. Primer sequences used are described in Table S2.

2.9 | Western blotting

Proteins were extracted from cultured cells using RIPA lysis buffer (Tris pH 8.0, 150 mM NaCl, 5 mM EDTA, 1% Triton, 0.5% Na-deoxycholate, 0.1% SDS) supplemented with a mix of protease inhibitors including AEBSF (30827-99-7, Sigma-Aldrich), PIC (05056489001, Roche), and anti-phosphatase (PhosSTOP, 04906837001, Roche). Cell lysates were subjected to SDS–polyacrylamide gel electrophoresis (SDS–PAGE) and transferred to a nitrocellulose membrane (GE Healthcare, UK). Membranes were blocked by incubation in Tris-buffered saline (TBS) buffer containing 0.1% Tween-20 and 5% non-fat dry milk or 1% bovine serum albumin (BSA) and further incubated overnight at 4°C with the primary antibodies described in Table S3. Bound antibodies were detected with horseradish peroxidase-conjugated mouse (P0447, Dako) or rabbit (P0448, Dako) IgG at the dilution of 1/10.000 and revealed with the Clarity Western ECL Substrate Kit (Biorad). Protein amounts were normalized with actin. Quantification and analyses were performed using ImageJ/FiJi software and R.

2.10 | Cell proliferation assay

Analysis of live cell proliferation was performed using the IncuCyte S3 Live-Cell Analysis System (Sartorius). Transfected LX-2 cells were seeded at a density of 4×10^3 cells/well in 96-well plates 24 h after siRNA transfection. After 6 h of incubation, culture media was replaced with fresh medium containing Nuclight Rapid Red Dye diluted at 1/1000 (NRR; 4717, Sartorius). Live cell proliferation was visualized every 4 h for 72 h using a 10× objective. Using the IncuCyte S3 Live-Cell analysis system software, cells were counted based on NRR staining and a proliferation index was calculated by dividing the cell number at each time point by the cell number at the beginning of the time course for each condition.

2.11 | Migration assay

Eighty hours after siRNA transfection, cells were cultured for 16 h in low serum (2%)-containing medium. Next, 8×10^4 transfected LX-2 cells were added in the top compartment of Boyden chambers in low serum (2%)-containing medium. The bottom compartment was filled with complete growth medium (10% FBS). Cells were allowed to migrate for 6 h at 37°C. To quantify migration, cells were mechanically removed from the upper side of the membrane using a cotton swab, and migrating cells on the lower side were fixed with 70% ethanol and stained with Hoechst-33342. Images were acquired using a TCS SP8 confocal microscope (Leica). Five representative images were analyzed for each insert. Each experiment was conducted in duplicate.

2.12 | xCELLigence assay

Cell spreading analysis was performed using the real-time cell analysis (RTCA) xCELLigence instrument (ACEA Biosciences). Ninety-six hours after siRNA transfection, LX-2 cells were seeded at a density of 2×10^4 cells/well in a 16-well E-Plate (Agilent). Cell index (CI) measurements

were taken every 5 min over a period of 6 h. The CI values were normalized to the mean of CI values of siCTRL cells at 6 h.

2.13 | Statistical analyses

Statistical analyses and graphs were performed using R. Statistical significances between groups were assessed by nonparametric or parametric tests as indicated in figure legends.

3 | RESULTS

3.1 | Characterization of an ECM-enriched signature associated with fibrosis

To characterize the matrisome in human liver fibrosis, we conducted an enrichment of extracellular matrix (ECM) proteins from human patient samples as previously described[15] using Naba's protocol.[14] Proteomic analyses identified 1131 proteins within 18 adjacent non-tumor tissue samples from patients with hepatocellular carcinoma. Using the NABA_MATRISOME_GSEA gene set (1020 genes) we identified 198 proteins present in the matrisome corresponding to 182 genes (Table S4). Among them, 16 exhibited differential protein expression across at least two fibrosis stages (Figure S1). With the exception of COL5A3, these proteins have all been previously detected in healthy liver using a similar extraction protocol.[19] The protein levels were either decreased or increased between F1 and F4 fibrosis stages. Three collagen proteins, COL4A1, COL5A3, and COL18A1, were found to be decreased, aligning with findings from a previous study using decellularization approaches.[6] Although increased expression of type XVIII collagen has been previously associated with liver fibrosis,[20,21] we observed its decrease with the progression of fibrosis in the ECM-enriched preparations. Using a comparable ECM purification approach, Baiocchini et al. also reported a reduction in COL18A1 in F4 stage.[6] Conversely, a group of proteins comprising INHBE, LTBP4, and VWF were increased in F4 stage. Some proteins such as CTSB and LAMA4 showed an increase restricted to F2 or F3 stages, while FBN1 displayed a decrease restricted to F3 samples. Remarkably, we observed an increase in the amounts of three members of the fibulin protein family, fibulin-2, -3, and -5 which were associated with fibrosis progression (Figure 1A). An accumulation of fibulin-5 protein levels was previously reported in HBV/HCV-associated hepatic fibrosis.[8] Additionally, increased mRNA expression of *FBLN5* and *EFEMP1* has recently been associated with liver fibrosis in patients with NAFLD.[22,23] Upon analyzing mRNA expression of *FBLN2*, *EFEMP1*, and *FBLN5* in non-malignant tissue adjacent to tumor from patients with hepatocellular carcinoma ($n = 50$), only *EFEMP1* mRNA expression was significantly increased in F4 compared to F1 samples (Figure 1B).

3.2 | Analysis of protein–protein interactions suggests functional specificities for fibulin-2, -3 and -5

To compare the potential functions of the three fibulins, we analyzed their protein partners using the Proteomics Standard Initiative Common Query Interface (PSICQUIC) webservice developed by the European Bioinformatics Institute.[16] As shown in supplementary information (Tables S5–S7), fibulin queries using gene names (*FBLN2*, *EFEMP1*, and *FBLN5*) resulted in 104, 377, and 305 interactions, respectively. Manual curation was required to eliminate redundant annotations and to select unique human protein–protein interactions (PPIs). The final list contains 43, 129, and 158 interacting proteins for FBLN2, EFEMP1, and FBLN5, respectively. As shown in Figure 2A,B, each fibulin is characterized by a specific PPI repertoire, with only 16 proteins being shared by all three fibulins. Among these 16 common proteins, 10 belong to the core matrisome. In addition to vitronectin (VTN), they comprise nine proteins contributing to the formation of elastic fibers involved in liver fibrosis[24] including five members of the microfibrillar associated proteins family (MFAP1, MFAP2, MFAP3, MFAP4, MFAP5), two fibrillins (FBN1 and FBN2), elastin (ELN) and elastin microfibril interfacer EMILIN1. To further explore each PPI network, we analyzed the over-representation of *biological_process* gene ontology (GO) terms associated with the network proteins. Although the three protein networks shared general GO terms such as *extracellular matrix organization* (Figure S2), clustering of ontologies using the affinity propagation method highlighted over-represented GO terms specific for each fibulin network (Figure 2C): *elastic fiber assembly* for FBLN5, *collagen-activated tyrosine kinase receptor signaling pathway* for FBLN2, and *response to endoplasmic reticulum stress* for EFEMP1. The critical role of FBLN5 in elastic fiber development has been previously demonstrated[25] while FBLN2 was associated with basement membrane stability[26,27] mediating cell adherence to collagen.[28] The association of the EFEMP1 PPI network with the GO term *response to endoplasmic reticulum stress* is attributed to a group of proteins including ANXA5, DNAJC10, PDIA4, P4HB, RCN1, SDF2L1, and TXNDC5. These proteins were previously identified

in a screen based on the overexpression of *EFEMP1* in an adenovirus-infected retinal pigment epithelium (RPE) cell line.[29] Since the overexpression of ECM proteins is known to be associated with ER stress[30] due to the mobilization of quality control in secretory pathways,[31] such a screen could therefore artificially over-represent interactions with specialized proteins involved in this quality control. Besides the GO term *response to endoplasmic reticulum stress*, our analysis revealed another interesting GO term that is *negative regulation of cell signaling and communication* suggesting specific functions for the EFEMP1 PPI network (Figure 2C).

Together our data demonstrate that even if fibulin-2, -3, and -5 are closely linked to ECM organization, the functional annotations of their respective PPI networks suggest that they have different roles. In order to explore these functional differences, we first investigated the cellular source of these fibulins in the liver.

3.3 | *FBLN2*, *EFEMP1*, and *FBLN5* are expressed in hepatic stellate cells

Taking advantage of single cell RNA-sequencing datasets from the liver Cell Atlas web site,[32] we analyzed cellular sources of *FBLN2*, *EFEMP1*, and *FBLN5* mRNA in the human liver. As shown in Figure 3A (left panel), *FBLN2* and *FBLN5* mRNAs exhibit a broader distribution among

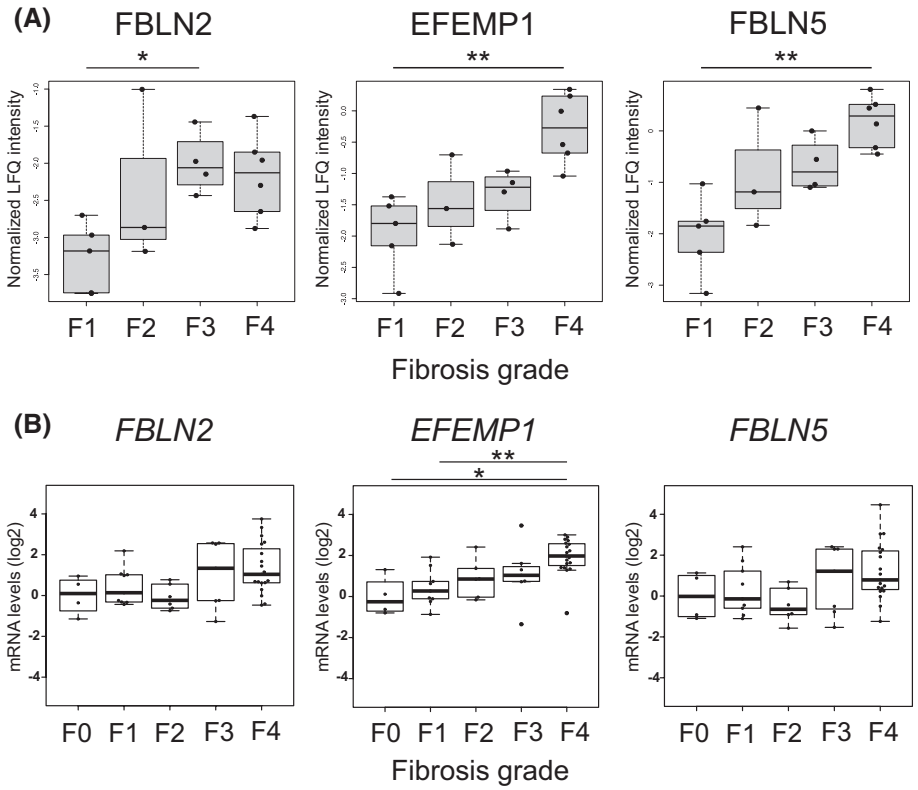

FIGURE 1 Expression of fibulins in human liver fibrosis. (A) Relative levels of fibulin-2, -3, and -5 proteins in the ECM-enriched extracts from human liver tissues at various fibrotic stages: F1 ($n=5$), F2 ($n=3$), F3 ($n=4$), and F4 ($n=6$). Extracellular matrix extraction was performed according to the standardized method of Naba[14] and extracts were analyzed by mass spectrometry. Normalized LFQ values were compared using a nonparametric Mann–Whitney test. Statistical significances were calculated using a nonparametric Mann–Whitney test. (B) *FBLN2*, *EFEMP1*, and *FBLN5* gene expression measured by RT-qPCR in human liver samples ($n=50$) at different fibrotic states: F0 ($n=4$), F1 ($n=10$), F2 ($n=7$), 7 F3 ($n=7$), and F4 ($n=22$)). Statistical differences were evaluated using a nonparametric Dunn test with an adjusted *p*-value. *$p<.05$, **$p<.01$.

FIGURE 2 Comparative analysis of protein–protein interaction (PPI) networks of fibulin-2 (FBLN2), fibulin-3 (EFEMP1), and fibulin-5 (FBLN5). (A) Graph representation of shared PPI networks for FBLN2, EFEMP1, and FBLN5 (pink nodes) using Cytoscape software. Proteins from the core matrisome are colored as green nodes and matrisome-associated proteins as blue nodes. (B) Venn diagram of PPIs. (C) Over-representation analysis of biological processes using the WEB-based Gene SeT AnaLysis Toolkit (we selected the affinity propagation tool that uses the R package apcluster to cluster gene sets).

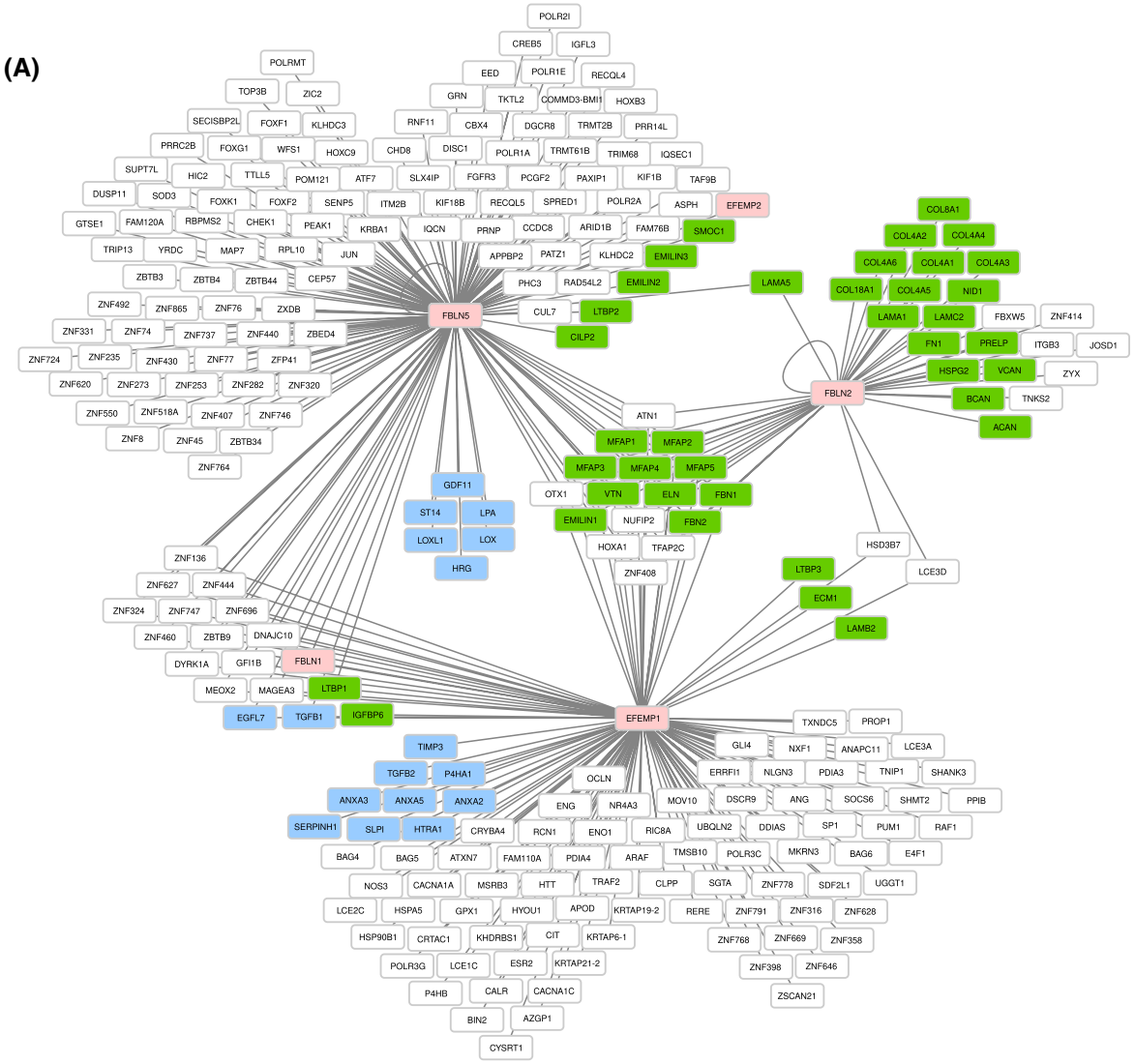
(A)
POLR2I
CREB5
IGFL3
POLRMT
EED
POLR1E
RECQL4
TOP3B
ZIC2
GRN
TKTL2
COMMD3-BMI1
HOXB3
SECISBP2L
FOXF1
KLHDC3
RNF11
CBX4
DGCR8
TRMT2B
PRR14L
PRRC2B
FOXG1
WFS1
HOXC9
CHD8
DISC1
POLR1A
TRMT61B
TRIM68
IQSEC1
SUPT7L
HIC2
TTLL5
POM121
ATF7
SLX4IP
FGFR3
PCGF2
PAXIP1
KIF1B
TAF9B
DUSP11
SOD3
FOXK1
FOXF2
SENP5
ITM2B
KIF18B
RECQL5
SPRED1
POLR2A
ASPH
EFEMP2
GTSE1
FAM120A
RBPMS2
CHEK1
PEAK1
KRBA1
IQCN
PRNP
CCDC8
ARID1B
FAM76B
SMOC1
TRIP13
YRDC
MAP7
RPL10
JUN
APPBP2
PATZ1
KLHDC2
EMILIN3
ZBTB3
ZBTB4
ZBTB44
CEP57
PHC3
RAD54L2
EMILIN2
LAMA5
ZNF492
ZNF865
ZNF76
ZXDB
FBLN5
CUL7
LTBP2
ZNF331
ZNF74
ZNF737
ZNF440
ZBED4
CILP2
ZNF724
ZNF235
ZNF430
ZNF77
ZFP41
ZNF620
ZNF273
ZNF253
ZNF282
ZNF320
ZNF550
ZNF518A
ZNF407
ZNF746
ZNF8
ZNF45
ZBTB34
ZNF764
COL8A1
COL4A2
COL4A4
COL4A6
COL4A1
COL4A3
COL18A1
COL4A5
NID1
LAMA1
LAMC2
FBXW5
ZNF414
FN1
PRELP
ITGB3
JOSD1
HSPG2
VCAN
ZYX
FBLN2
BCAN
TNKS2
ACAN
ATN1
MFAP1
MFAP2
MFAP3
MFAP4
MFAP5
GDF11
OTX1
VTN
ELN
FBN1
ST14
LPA
EMILIN1
NUFIP2
FBN2
LOXL1
LOX
HOXA1
TFAP2C
HRG
ZNF408
HSD3B7
LTBP3
LCE3D
ECM1
ZNF136
LAMB2
ZNF627
ZNF444
ZNF324
ZNF747
ZNF696
ZNF460
ZBTB9
DNAJC10
DYRK1A
GFI1B
FBLN1
MEOX2
MAGEA3
LTBP1
EGFL7
TGFB1
IGFBP6
EFEMP1
TXNDC5
PROP1
TIMP3
GLI4
NXF1
ANAPC11
LCE3A
TGFB2
P4HA1
ERRFI1
NLGN3
PDIA3
TNIP1
SHANK3
OCLN
ANXA3
ANXA5
ANXA2
ENG
NR4A3
MOV10
DSCR9
ANG
SOCS6
SHMT2
PPIB
SERPINH1
SLPI
HTRA1
CRYBA4
RCN1
ENO1
RIC8A
UBQLN2
DDIAS
SP1
PUM1
RAF1
BAG4
BAG5
ATXN7
FAM110A
PDIA4
ARAF
TMSB10
POLR3C
MKRN3
BAG6
E4F1
NOS3
CACNA1A
MSRB3
HTT
TRAF2
CLPP
SGTA
ZNF778
SDF2L1
UGGT1
LCE2C
HSPA5
GPX1
HYOU1
APOD
KRTAP19-2
RERE
ZNF791
ZNF316
ZNF628
HSP90B1
CRTAC1
KHDRBS1
CIT
KRTAP6-1
ZNF768
ZNF669
ZNF358
POLR3G
LCE1C
ESR2
KRTAP21-2
ZNF398
ZNF646
P4HB
CALR
CACNA1C
ZSCAN21
BIN2
AZGP1
CYSRT1
(B)
EFEMP1
FBLN2
FBLN5
94
2
24
16
17
1
119
(C)
EFEMP1
FDR ≤ 0.05
FDR > 0.05
response to reticulum stress
extracellular matrix organization
negative regulation of cell communication
Enrichment ratio
FBLN2
FDR ≤ 0.05
FDR > 0.05
collagen-activated tyrosine kinase receptor signaling pathway
extracellular structure organization
blood vessel morphogenesis
Enrichment ratio
FBLN5
FDR ≤ 0.05
FDR > 0.05
elastic fiber assembly
extracellular matrix organization
negative regulation of transcription, DNA-templated
Enrichment ratio

liver cells compared to *EFEMP1*. *FBLN2* mRNA is mainly expressed in stromal and endothelial cells, but is also present in immune cells, particularly in type-2 conventional dendritic cells (cDC2) and macrophages. Similarly, *FBLN5* expression is mainly associated with stromal cells, but is also weakly present in endothelial cells. *FBLN5* is also expressed in the two major liver cell types: hepatocytes and cholangiocytes (biliary epithelial cells) as well as in immune cells including natural killers (NK and NKT) and T cells. Like *FBLN5*, *EFEMP1* is also expressed in stromal cells and cholangiocytes, but it is absent in immune cells and endothelial cells. Overall, *FBLN2*, *EFEMP1*, and *FBLN5* transcripts are predominantly expressed in stromal cells. Noteworthy, stromal cells include fibroblasts, hepatic stellate cells (HSCs) and vascular smooth muscle cells (VSMCs) as shown by selecting the *human CD45⁻ cell subpopulation* defined in the Liver Cell Atlas (Figure 3A, right panel). This subpopulation also contains hepatocytes, cholangiocytes, and endothelial cells (ECs; Central vein ECs, Portal vein ECs, Liver Sinusoidal ECs). Based on this *in silico* analysis, we concluded that *FBLN2*, *EFEMP1*, and *FBLN5* are mainly expressed by fibroblasts and quiescent HSCs in the normal liver. Due to the critical role of activated HSCs in liver fibrosis, we studied the expression of *FBLN2*, *EFEMP1*, and *FBLN5* in primary cultures of activated human HSCs and in the human HSC cell line, LX-2. Compared to human hepatocytes, cultured human HSCs express higher levels of *FBLN2*, *EFEMP1*, and *FBLN5* mRNA (Figure 3B). Examining LX-2 cells, we found that FBLN2 and EFEMP1 mRNA were expressed at a higher level than FBLN5 mRNA (Figure 3C). Consistently, fibulin 2 and fibulin 3 proteins are highly synthesized by LX-2 cells, while fibulin 5 remains barely detectable in LX2 cell extracts (Figure S3). When LX-2 cells were treated with TGF-β or IL-1β, we observed a strong induction of *FBLN5* mRNA expression upon TGF-β stimulation and a marked decrease in *EFEMP1* mRNA expression upon IL-1β stimulation, while *FBLN2* mRNA expression was not affected, indicating differential regulation of the three fibulins in LX-2 cells (Figure 3D). As controls, we confirmed that expression levels of *MMP9* and *COL1A2* were upregulated by IL-1β and TGF-β treatments, respectively, as previously described.[33,34]

3.4 | Silencing of *EFEMP1* does not affect TGF-β response in hepatic stellate cells

Among GO terms associated with EFEMP1 PPI networks (Figure S2), we identified *negative regulation of cell signaling*. Consistently, the negative effect of fibulin-3 on TGF-β signaling has been previously reported through inhibition of its interaction with TGF-β receptor 1 (TGFBR1).[35,36] Of note, TGFBR1 was not identified as a member of the EFEMP1 PPI network using PSICQUIC, suggesting that the databases are incomplete (Table S6). Due to the critical role of TGF-β in liver fibrosis, we analyzed the effect of *EFEMP1* knockdown on the cell response to TGF-β and compared results to those of *FBLN2* knockdown. From three different siRNAs, we selected siEFEMP1 number 2 as the most efficient and specific on EFEMP1 expression (Figure S4A). As shown in Figure 4A, transfection of siEFEMP1 and siFBLN2 in LX-2 cells reduced protein amounts of fibulin-3 and fibulin-2, respectively. Despite efficient depletion of both *FBLN2* and *EFEMP1* mRNAs by their corresponding siRNAs (Figure S4B) the lesser effect of fibulin-3 reduction at the protein level could possibly be due to greater stability of the protein.

To analyze the effect of *EFEMP1* silencing on the cellular response to TGF-β, we measured the expression of TGF-β-targeted genes including *FBLN5* and *PAI1*. As shown in Figure 4B, after 96 h of *EFEMP1* and *FBLN2* silencing in LX-2 cells, the induction of TGF-β responsive genes was not affected. Consistent with this absence of effect of *EFEMP1* and *FBLN2* silencing on the induction of TGF-β-dependent gene expression, we observed no changes in activation of TGF-β-dependent signaling pathways. Specifically, phosphorylation of SMAD2 and SMAD3 (Figure 4C) induced by TGF-β stimulation was unchanged in silenced cells compared to controls, suggesting that SMAD-dependent TGF-β signaling pathways were unaffected.

3.5 | Silencing of *EFEMP1* but not *FBLN2* induces a defect in the organization of stress fibers

EFEMP1-silenced cells cultured for 96 h displayed progressive changes in their phenotype compared to control

FIGURE 3 *FBLN2*, *EFEMP1*, and *FBLN5* expression in liver cells. (A) Analysis of RNAseq data from the Liver Cell Atlas (https://liver cellatlas.org/).[32] Expression levels are represented as Log2 (transcripts per million) in all human liver cells (left panels) and in human CD45⁻ cells (right panels). (B) Fibulin gene expression measured by RT-qPCR in cultured primary human hepatocytes (HH) and hepatic stellate cells (HSC) ($n = 5$). (C) Gene expression of fibulins measured by RT-qPCR in the human HSC cell line, LX-2 ($n = 4$). (D) Gene expression of fibulins measured by RT-qPCR in cultured LX-2 cells stimulated with TGF-β (5 ng/mL) or IL-1β (3 ng/mL) compared to untreated cells (control) ($n = 4$). Results are from five (B) or four (C and D) independent experiments. Statistical differences were evaluated using a nonparametric Mann–Whitney test. *$p < .05$, **$p < .01$.

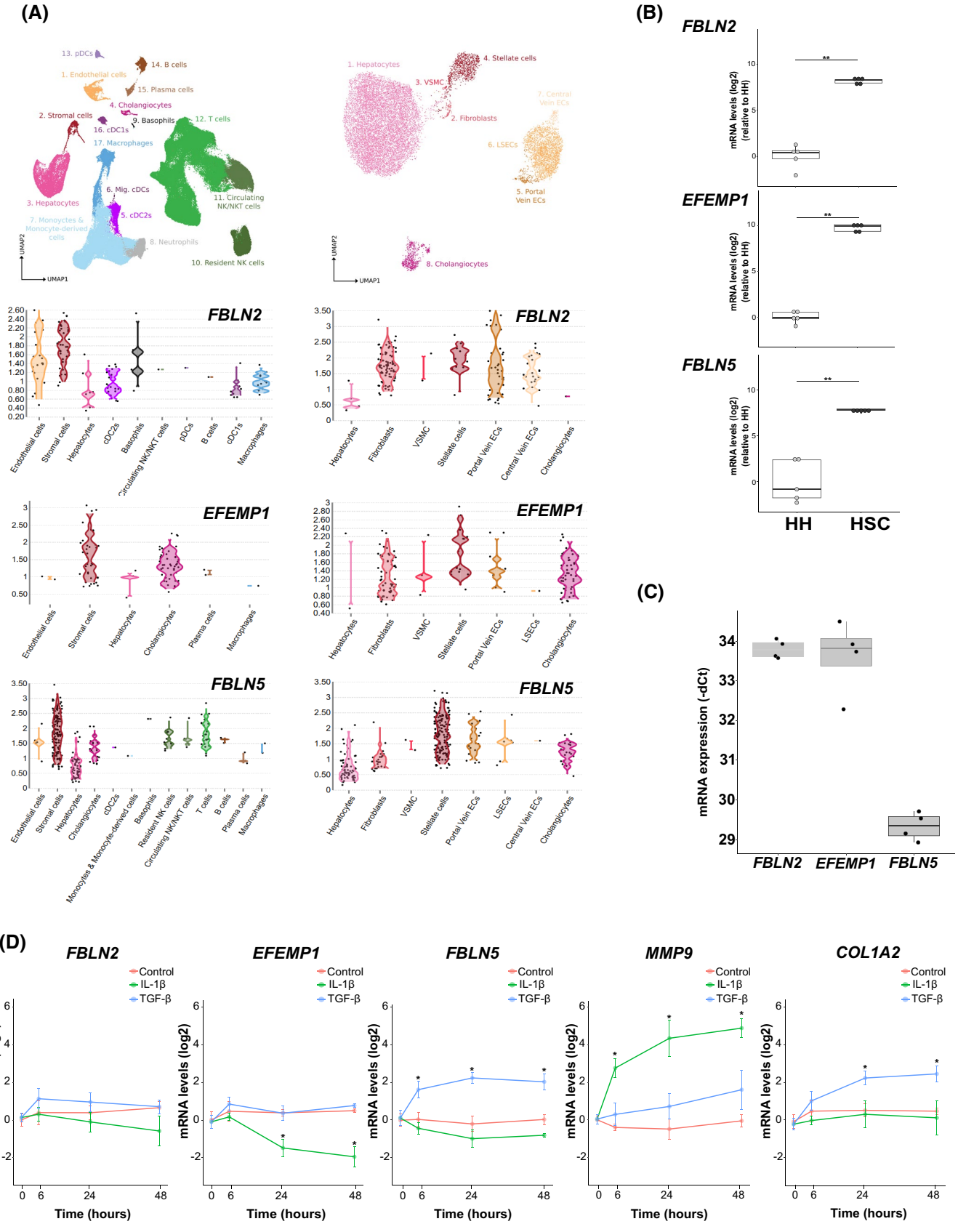

cells (Figure S5). In addition, staining of F-actin using phalloidin showed that the organization of actin filaments was dramatically altered in *EFEMP1*-silenced cells, while *FBLN2*-silenced cells were less affected (Figure 5A). F-actin is a structural component of stress fibers that exert direct mechanical tensions on the nuclei.[37–39] Measurement

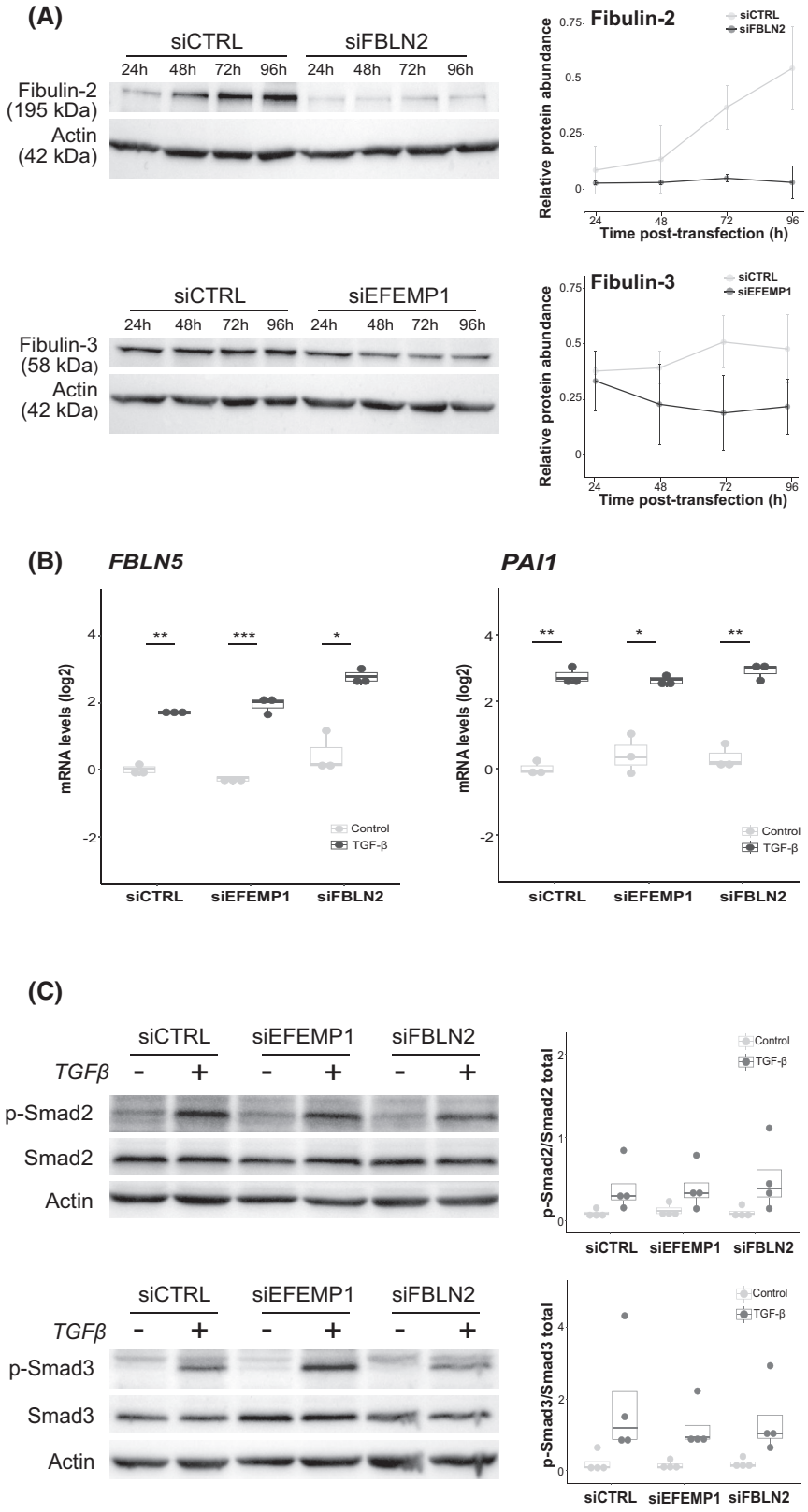

FIGURE 4 Silencing of *EFEMP1* does not affect TGF-β-dependent cell signaling in LX-2 cells. (A) LX-2 cells were transfected with a control siRNA (siCTRL), or an siRNA against *EFEMP1* (siEFEMP1) or *FBLN2* (siFBLN2) for the indicated times (24–96 h). The efficiency of RNA interference was measured by western blotting. Results are from three independent experiments. (B) Expression levels of TGF-β-dependent genes (*FBLN5* and *PAI1*) were measured by RT-qPCR in LX-2 cells transfected with the indicated siRNAs and treated or not with TGF-β (5 ng/mL) for 16 h ($n = 3$). (C) Analysis of TGF-β-induced SMAD activation by Western blot, after 16 h of stimulation ($n = 4$). Results are from three (B) or four (C) independent experiments and statistical differences were evaluated using a parametric paired *t*-test. *$p < .05$, **$p < .01$, ***$p < .001$.

of nuclear projected areas can therefore be used to assess the effects of actin disorganization on stress fiber tension. In line with previous observations, TGF-β treatment induced stress fibers, which can be observed by phalloidin staining (Figure 5A) and quantified by measuring the projected areas of the nucleus (Figure 5B). Nuclei areas were significantly reduced in *EFEMP1*-silenced cells regardless of the type of surface on which the cells were cultured (plastic or collagen-coated dishes) while we observed no significant changes in *FBLN2*-silenced cells. Consistent with these results, the actin network and the tension forces exerted on nuclei tend to be reinforced when EFEMP1 is overexpressed (Figure S6). Importantly, nuclear areas were increased after TGF-β treatment in both control and silenced cells (Figure 5), in line with the observation that the response to TGF-β *per se* was not affected by *EFEMP1* or *FBLN2* silencing in LX-2 cells (Figure 4). Of note, the effect of TGF-β on nuclear sizes was more marked when cells were cultured on collagen-coated surfaces (Figure 5B, lower panel). As a control, we checked that the total DNA content was not affected, indicating that the changes in nuclei projected areas primarily reflected changes in nuclear shape (Figure S7). Together, these results demonstrate that *EFEMP1* silencing reduces the tensions exerted by the actin cytoskeleton on the nuclei.

3.6 | Silencing of *EFEMP1* and *FBLN2* differentially affects focal adhesions, FAK phosphorylation, and cell migration

Given the functional link between stress fibers and focal adhesions,[40] we investigated whether the observed disorganization of the actin network in *EFEMP1*-silenced cells was associated with changes in the organization of focal adhesions. To this end, we performed immunostaining of the focal adhesion component paxillin in LX-2 cells. As shown in Figure 6A, the number of paxillin-positive foci

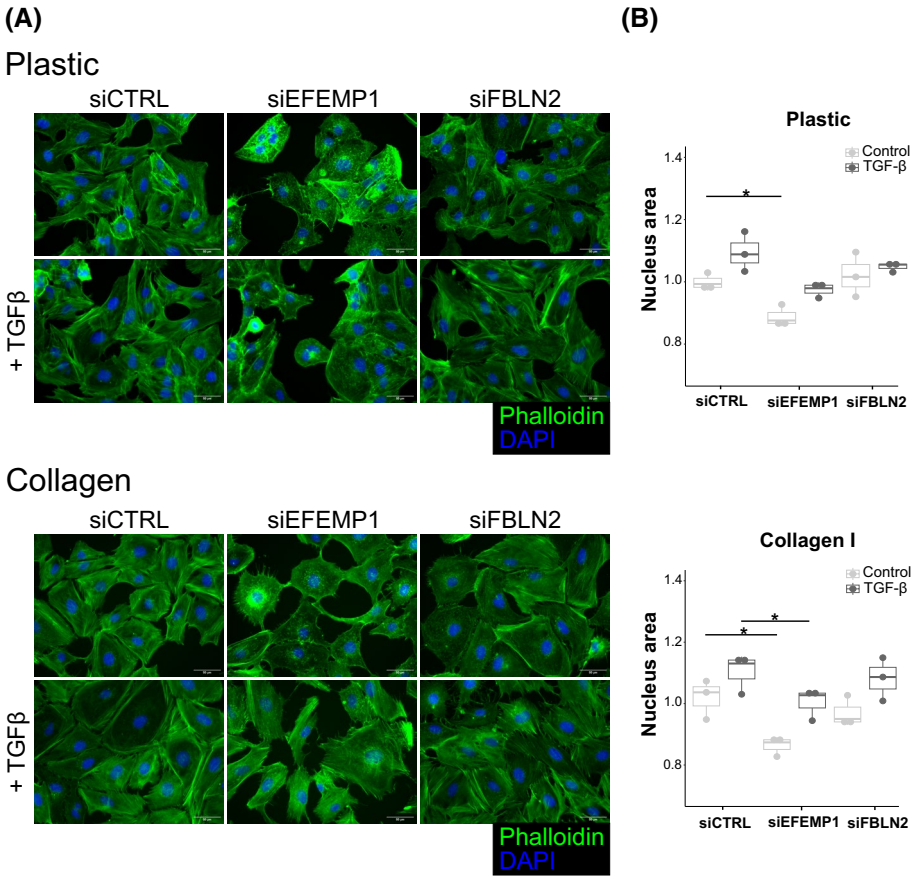

FIGURE 5 Silencing of *EFEMP1*, but not *FBLN2*, impairs the organization of stress fibers. LX-2 cells transfected with the indicated siRNAs, and treated or not with TGF-β (5 ng/mL for 16 h) were cultured on uncoated (plastic) or type I collagen (Collagen I)-coated plates. (A) After 96 h of culture, cells were fixed and stained with phalloidin-Alexa-Fluor-488 for F-actin detection. Nuclei were counterstained with Hoechst-33342. Representative fields of three independent experiments are shown. (B) Average projected areas of nuclei from three independent experiments were measured and used to compare nuclear sizes. Statistical significances were evaluated using a parametric paired *t*-test, $*p < .05$.

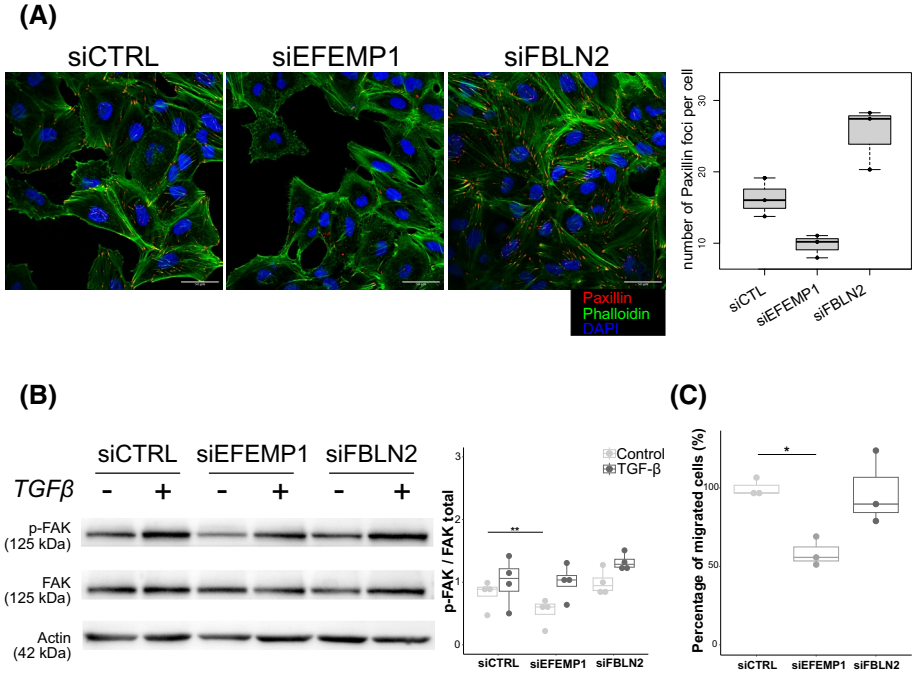

FIGURE 6 Silencing of *EFEMP1* and *FBLN2* differentially affects focal adhesion, FAK phosphorylation, and cell migration. (A) LX-2 cells transfected with the indicated siRNA were cultured on uncoated (plastic) plates. After 96 h of culture, cells were fixed and immunostained with anti-paxillin. F-actin was stained using phalloidin-Alexa-Fluor-488 and nuclei were counterstained with Hoechst-33342 ($n = 3$). Average numbers of paxillin-positive foci per cell were scored from at least five representative fields per experiment. Representative fields of one of three independent experiments are shown. Scale bar: 50 μm. (B) FAK phosphorylation (relative to total FAK protein) was measured by western blot in control or silenced cells treated or not by TGF-β (5 ng/mL) for 16 h ($n = 4$). Results are from four independent experiments and statistical differences were evaluated using a parametric paired *t*-test. (C) Migration was measured using a transwell assay. Cells that have migrated are shown as a percentage relative to siCTRL cells. Statistical significances were evaluated from three independent experiments using a nonparametric Mann–Whitney test. $^*p < .05$, $^{**}p < .01$.

per cell was lower in *EFEMP1*-silenced cells when compared with control cells. By contrast, we observed an increase in the number of paxillin-positive focal adhesions in *FBLN2*-silenced cells. In line with these observations, phosphorylation of focal adhesion kinase (FAK) was diminished in *EFEMP1*-silenced cells compared to control and *FBLN2*-silenced cells (Figure 6B). In addition, we observed that TGF-β treatment induced FAK phosphorylation in control cells in line with the known effect of TGF-β on FAK activation in HSCs.[41] This induction of FAK phosphorylation upon TGF-β treatment was also observed in both *EFEMP1*- and *FBLN2*-silenced cells, consistent with our above observation that the response to TGF-β was not affected by *FBLN2* or *EFEMP1* silencing.

Focal adhesions are involved in both cell adhesion and migration.[42] Using xCELLigence real-time cell analysis, we showed that *EFEMP1* silencing did not affect the early stages of cell spreading and attachment, whereas the impedance signal was significantly higher at 6 h after seeding of *FBLN2*-silenced cells when compared to control cells (Figure S8). Consistent with the role of focal adhesions and FAK signaling in cell migration, we further observed a decrease in the migration of *EFEMP1*-silenced cells compared with control and *FBLN2*-silenced cells (Figure 6C). Finally, using real-time live-cell imaging, we found that cell proliferation was not affected by either *EFEMP1* or *FBLN2* siRNA (Figure S9).

3.7 | Silencing of *EFEMP1* modulates fibronectin network integrity

FAK activation plays an essential role in cell migration driven by β1 integrin signaling.[43,44] Moreover, previous studies have demonstrated reciprocal cross-talk between the spatial distribution of focal adhesions and fibronectin organization, mediated by the fibronectin receptor α5β1 integrin.[45] We therefore studied the distribution of both fibronectin and α5β1 integrin in *EFEMP1*-silenced cells. We observed significant changes in the organization of the fibronectin network at the cell surface of *EFEMP1*-silenced cells (Figure 7A) consistent with the established role of FAK in the allocation and organization of fibronectin (*FN1*) matrix.[46] Compared to control cells and *FBLN2*-silenced cells, both the length (Figure 7B) and

number (Figure 7C) of fibronectin fibers were decreased in *EFEMP1*-silenced cells. Since the cells were cultured on uncoated plastic dishes, these changes can be attributed to fibronectin produced by the LX-2 cells. We therefore analyzed fibronectin production and found no significant alteration in mRNA expression (Figure 7D) but a reduced amount of protein in *EFEMP1*-silenced cells (Figure 7E,F) suggesting that fibronectin production and/or deposition was impaired in *EFEMP1*-silenced cells. In correlation with these observations, we observed that the spatial distribution of the fibronectin receptor α5β1 integrin was as well altered in *EFEMP1*-silenced cells compared with control and *FBLN2*-silenced cells (Figure S10).

4 | DISCUSSION

As described by A. Naba in a recent review, proteomic analyses of the extracellular matrix face a number of challenges, mainly related to the biochemical properties of its components and their complex assembly.[47] Although there are commonalities between ECM enrichment by sequential purification and decellularization protocols, each of these approaches results in slightly different proteomic profiles, which may also vary with the biological samples analyzed.[48] In the present study, we used the enrichment protocol developed by Naba et al.[14], which has previously been used for human liver samples[19] and has proven to be more appropriate for studying the liver matrisome.[48] In line with this, our results show partial overlap with previous liver fibrosis proteomes. We have identified three members of the fibulin family of proteins that have previously been reported in proteomic analyses of liver fibrosis. Based on decellularized methods, increased amounts of fibulin-2,-3, and -5 were reported in human cirrhotic structures compared to healthy scaffolds[9] and fibulin-3 and -5 were increased in advanced liver fibrosis from patients with HCV.[6] Of note, a label-free proteomics discovery study identified an association of fibulin-5 with liver fibrosis in biopsied tissue samples from patients with hepatitis B or C.[8] Whatever the experimental approach, these three fibulins have commonly been identified as markers of fibrosis, but their role in liver fibrosis is poorly documented. Fibulin-2 was initially identified as a marker of portal myofibroblasts.[49,50] However, a recent study identified a new sub-population of highly profibrotic and proinflammatory HSCs that strongly express *Fbln2* in an alcoholic hepatitis mice model[51] suggesting that fibulin-2 is involved in both portal and sinusoidal fibrosis. Through binding to elastin, fibulin-5 has been shown to be a major regulator of elastic fiber assembly[25] and to contribute to the deposition of elastic fibers in cirrhotic liver.[24] Fibulin-3 was recently identified as a seric marker of fibrosis in the context of metabolic dysfunction-associated steatotic liver disease.[52] Unlike fibulin-2 and fibulin-5, fibulin-3 does not interact with basement membrane components such as type IV collagen or tropoelastin[53] and our own analysis of PPI networks clearly demonstrates that fibulin-3 is involved in different biological processes (Figure 2). In chronic liver diseases, *EFEMP1* overexpression was shown to inhibit the growth and migration of hepatocellular carcinoma cells,[54,55] however, the role of fibulin-3 in liver fibrosis was never explored.

In the present work, we showed that fibulin-3 plays a critical role in HSC migration and adhesion signaling, thereby contributing to regulate HSC functions. Unlike *FBLN2*-silenced cells, *EFEMP1*-silenced cells exhibited a default in stress fiber maturation associated with the loss of focal adhesions. Cells are known to use their focal adhesions to apply traction forces on the ECM and migrate.[56] Consistent with this, we also observed a decrease in the migration of *EFEMP1*-silenced cells. Interestingly, silencing of fibulin-3 did not affect the early steps of cell spreading, suggesting compensation by other adhesion systems. We demonstrated that fibronectin fibers at the cell surface are disorganized upon *EFEMP1* silencing in LX-2 cells, suggesting that fibulin-3 is involved in the organization and/or stabilization of the fibronectin network involved in cell–matrix interactions.

Consistent with an implication in the organization of the matrix network, depletion of *EFEMP1* expression has been shown to reduce the formation of collagen VI filaments in retinal pigmented epithelial cells,[57] and *Efemp1* null mice subjected to myocardial infarction exhibit less collagen deposition post-injury, associated with abnormal collagen fiber alignment.[58] Overexpression of *EFEMP1* in trabecular meshwork cells disturbs the fibronectin network at the cell surface, affecting their morphology by reducing intracellular actin stress fiber formation.[59] As suggested by Livingstone et al.,[60] the influence of fibulin-3 on fibrillar matrix integrity might be indirect, through interaction with other molecules such as TIMP-3.[61] Of note, overexpression of *EFEMP1* in endothelial cells is associated with both an increase in expression of TIMP-3 and an inhibition of metalloprotease activities, leading to an alteration of matrix integrity and cell migration.[62] We also analyzed *TIMP-3* expression in LX-2 cells after siRNA transfection and observed decreased *TIMP-3* mRNA and protein levels in *EFEMP1*-silenced cells compared to control and *FBLN2*-silenced cells (Figure S11), suggesting a role for fibulin-3 in the control of fibronectin remodeling through the regulation of proteases. According to previous observations,[45] this remodeling could in turn affect FAK activity and the distribution of focal adhesion, with consequences for cell adhesion and migration.

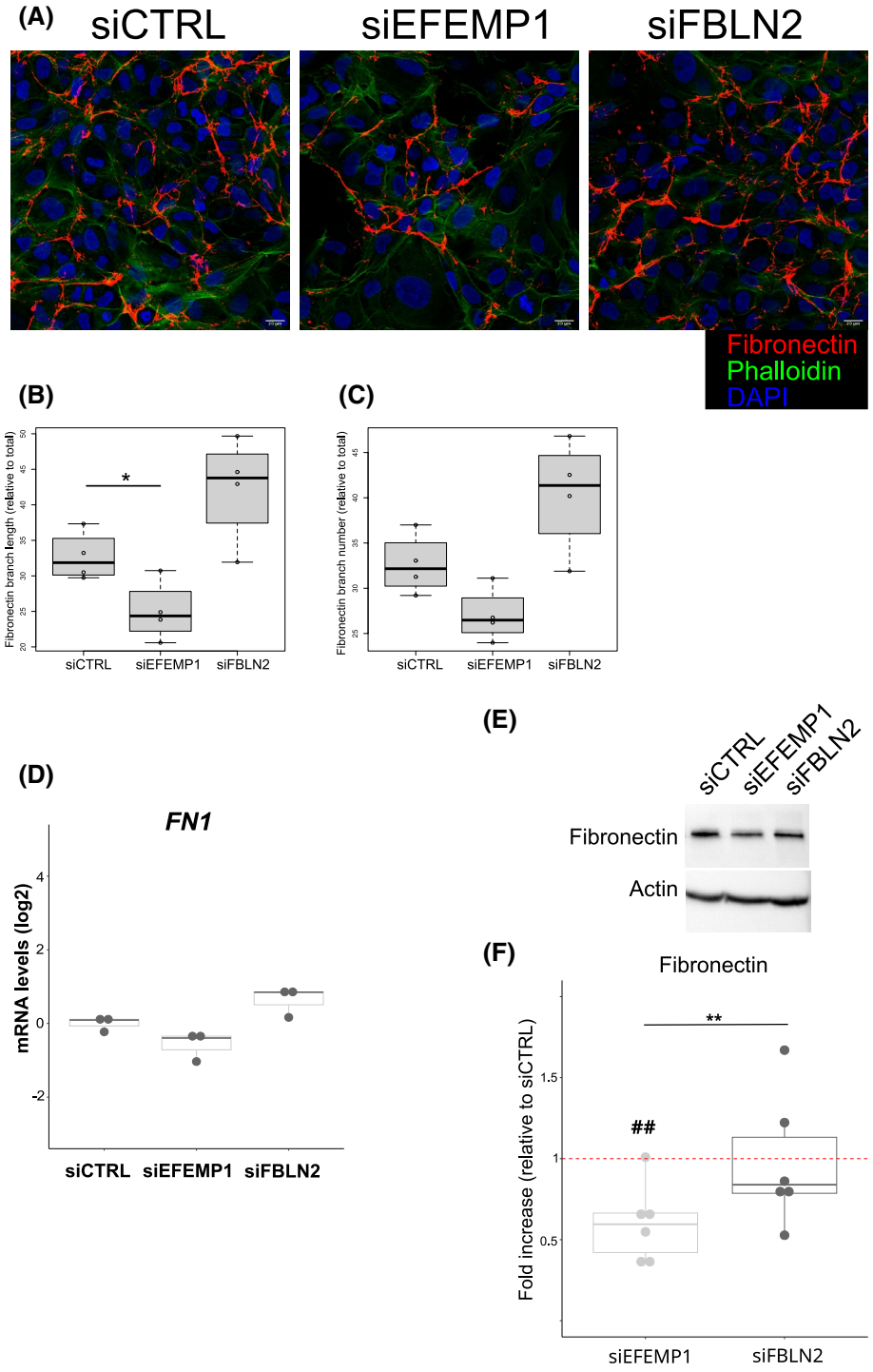

FIGURE 7 Fibulin-3 silencing alters the integrity of the fibronectin network. LX-2 cells transfected with the indicated siRNAs were cultured on uncoated (plastic) plates. (A) After 96 h of culture, cells were fixed and immunostained with an anti-fibronectin antibody. Actin fibers were stained using phalloidin-Alexa-Fluor-488 and nuclei with Hoechst-33342. Fields representative of three independent experiments are shown. Scale bar: 20 μm. Average length (B) and number (C) of fibronectin fibers from four independent experiments were calculated from at least 10 representative fields per experiment. (D) Gene expression level of *FN1* was measured by RT-qPCR (three independent experiments). (E, F) Protein amount was quantified by western blot. (E) Representative image and (F) quantification of six independent experiments relative to the value in cells transfected with control siRNAs (dotted line). Statistical significances were evaluated using a parametric paired *t*-test for fibronectin branch lengths, mRNA and protein level quantification, and a nonparametric Mann–Whitney test for fibronectin branch numbers. $^{*}p < .05$, $^{**}p < .01$, $^{\#\#}p < .01$.

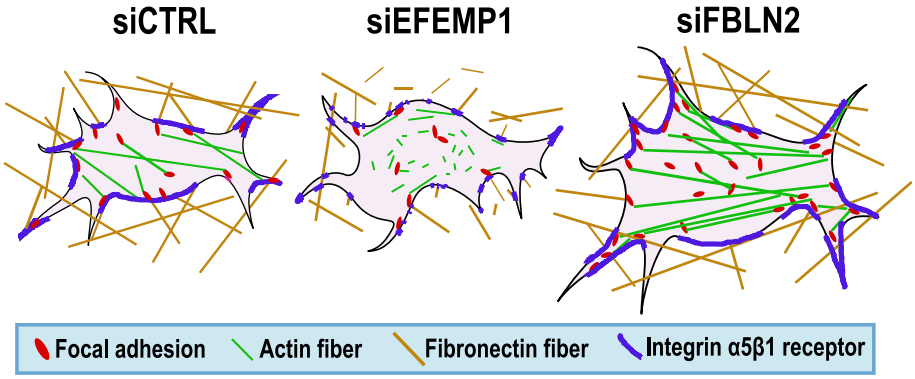

FIGURE 8 Schematic representation of *EFEMP1*- and *FBLN2*-silenced cells. *EFEMP1*-silenced cells show a maturation defect of stress fibers (green filaments) associated with a partial loss of focal adhesions (red dots), an altered fibronectin network (yellow filaments) at the cell surface and an impaired distribution of its receptor, integrin α5β1 (purple lines). In contrast, *FBLN2*-silenced cells show a denser actin network accompanied by a greater number of focal adhesions without significant alteration of fibronectin organization.

In conclusion, our proteomic analysis, in line with previous studies, confirmed an association of fibulin-2, -3 and -5 with liver fibrosis. While the functional role of fibulin-3 in liver fibrosis has remained unclear, our study is the first to demonstrate its impact on focal adhesion dynamics in hepatic stellate cells, likely by promoting cell–matrix interactions through remodeling fibronectin networks (Figure 8). Given the role of focal adhesion dynamics in cell motility, and the prominence of HSC migration in the response to liver injury, these observations highlight a new dimension of fibulin-3's role in liver fibrosis.

AUTHOR CONTRIBUTIONS

Célia Thomas, Fidaa Bouezzedine, Dominique Bonnier, and Vincent Legagneux performed the experimental studies. Célia Thomas, Fidaa Bouezzedine, Vincent Legagneux, and Nathalie Théret were involved in drafting and revising the manuscript. Vincent Legagneux and Nathalie Théret supervised the study and performed the bioinformatic analyses. All the authors have reviewed and approved the final manuscript.

ACKNOWLEDGMENTS

The authors thank the Centre de Ressources Biologiques de Rennes (CHRU Pontchaillou) for providing human tissue samples, and Dr. Bruno Turlin for clinical pathology analyses. Histopathological analyses were performed at the HistoPathology of High Precision facility (H2P2) and cell analyses at the Microscopy Rennes imaging center (Mric) and at the Imaging for Analysis of Cell Content facility (ImPACCell), hosted at UMS Biosit (INSERM UMS 018, CNRS UMS3480). The authors thank Dr. Alexandra Naba for fruitful discussion and Dr. Catherine Lavau (INSERM U1085, University of Rennes) for proofreading the manuscript.

FUNDING INFORMATION

This work was supported by the Institut National de la Santé et de la Recherche Médicale (INSERM), Université de Rennes, la Ligue Nationale Contre le Cancer, and the Région Bretagne.

DISCLOSURES

The authors declare no potential conflicts of interest.

DATA AVAILABILITY STATEMENT

The data that support the findings of this study are available in the Materials and Methods, Results, and/or Supplemental Material of this article.

ORCID

Vincent Legagneux https://orcid.org/0000-0002-1417-6678
Nathalie Théret https://orcid.org/0000-0002-5857-7828
Fidaa Bouezzedine https://orcid.org/0009-0006-7964-5603
Célia Thomas https://orcid.org/0009-0000-1775-3242

REFERENCES

1. Devarbhavi H, Asrani SK, Arab JP, Nartey YA, Pose E, Kamath PS. Global burden of liver disease: 2023 update. *J Hepatol*. 2023;79:516-537.
2. GBD 2017 Cirrhosis Collaborators. The global, regional, and national burden of cirrhosis by cause in 195 countries and territories, 1990–2017: a systematic analysis for the Global Burden of Disease Study 2017. *Lancet Gastroenterol Hepatol*. 2020;5:245-266.
3. Naba A, Clauser KR, Hoersch S, Liu H, Carr SA, Hynes RO. The matrisome: in silico definition and in vivo characterization by proteomics of normal and tumor extracellular matrices. *Mol Cell Proteomics*. 2012;11:M111.014647.

4. Hynes RO, Naba A. Overview of the matrisome—an inventory of extracellular matrix constituents and functions. *Cold Spring Harb Perspect Biol*. 2012;4:a004903.
5. Diamond DL, Jacobs JM, Paeper B, et al. Proteomic profiling of human liver biopsies: hepatitis C virus-induced fibrosis and mitochondrial dysfunction. *Hepatology*. 2007;46:649-657.
6. Baiocchini A, Montaldo C, Conigliaro A, et al. Extracellular matrix molecular remodeling in human liver fibrosis evolution. *PLoS One*. 2016;11:e0151736.
7. Mölleken C, Sitek B, Henkel C, et al. Detection of novel biomarkers of liver cirrhosis by proteomic analysis. *Hepatology*. 2009;49(4):1257-1266. doi:10.1002/hep.22764
8. Bracht T, Schweinsberg V, Trippler M, et al. Analysis of disease-associated protein expression using quantitative proteomics—fibulin-5 is expressed in association with hepatic fibrosis. *J Proteome Res*. 2015;14:2278-2286.
9. Mazza G, Telese A, Al-Akkad W, et al. Cirrhotic human liver extracellular matrix 3D scaffolds promote Smad-dependent TGF-β1 epithelial mesenchymal transition. *Cells*. 2019;9:E83.
10. Daneshgar A, Klein O, Nebrich G, et al. The human liver matrisome—proteomic analysis of native and fibrotic human liver extracellular matrices for organ engineering approaches. *Biomaterials*. 2020;257:120247.
11. Massey VL, Dolin CE, Poole LG, et al. The hepatic "matrisome" responds dynamically to injury: characterization of transitional changes to the extracellular matrix in mice. *Hepatology*. 2017;65:969-982.
12. Klaas M, Kangur T, Viil J, et al. The alterations in the extracellular matrix composition guide the repair of damaged liver tissue. *Sci Rep*. 2016;6:27398.
13. Wu Y, Cao Y, Xu K, et al. Dynamically remodeled hepatic extracellular matrix predicts prognosis of early-stage cirrhosis. *Cell Death Dis*. 2021;12:163.
14. Naba A, Clauser KR, Hynes RO. Enrichment of extracellular matrix proteins from tissues and digestion into peptides for mass spectrometry analysis. *J Vis Exp*. 2015;101:e53057. doi:10.3791/53057
15. Azar F, Courtet K, Dekky B, et al. Integration of miRNA-regulatory networks in hepatic stellate cells identifies TIMP3 as a key factor in chronic liver disease. *Liver Int*. 2020;40:2021-2033. doi:10.1111/liv.14476
16. Aranda B, Blankenburg H, Kerrien S, et al. PSICQUIC and PSISCORE: accessing and scoring molecular interactions. *Nat Methods*. 2011;8:528-529.
17. Le Pabic H, Bonnier D, Wewer UM, et al. ADAM12 in human liver cancers: TGF-beta-regulated expression in stellate cells is associated with matrix remodeling. *Hepatology*. 2003;37:1056-1066.
18. Zhang R-M, Kumra H, Reinhardt DP. Quantification of extracellular matrix fiber systems related to ADAMTS proteins. *Methods Mol Biol*. 2020;2043:237-250.
19. Naba A, Clauser KR, Whittaker CA, Carr SA, Tanabe KK, Hynes RO. Extracellular matrix signatures of human primary metastatic colon cancers and their metastases to liver. *BMC Cancer*. 2014;14:518.
20. Jia JD, Bauer M, Sedlaczek N, et al. Modulation of collagen XVIII/endostatin expression in lobular and biliary rat liver fibrogenesis. *J Hepatol*. 2001;35:386-391.
21. Musso O, Rehn M, Saarela J, et al. Collagen XVIII is localized in sinusoids and basement membrane zones and expressed by hepatocytes and activated stellate cells in fibrotic human liver. *Hepatology*. 1998;28:98-107.
22. Pantano L, Agyapong G, Shen Y, et al. Molecular characterization and cell type composition deconvolution of fibrosis in NAFLD. *Sci Rep*. 2021;11:18045.
23. He W, Huang C, Zhang X, et al. Identification of transcriptomic signatures and crucial pathways involved in non-alcoholic steatohepatitis. *Endocrine*. 2021;73:52-64.
24. Kanta J. Elastin in the liver. *Front Physiol*. 2016;7:491.
25. Yanagisawa H, Davis EC, Starcher BC, et al. Fibulin-5 is an elastin-binding protein essential for elastic fibre development in vivo. *Nature*. 2002;415:168-171.
26. Ibrahim AM, Sabet S, El-Ghor AA, et al. Fibulin-2 is required for basement membrane integrity of mammary epithelium. *Sci Rep*. 2018;8:14139.
27. Longmate WM, Monichan R, Chu M-L, Tsuda T, Mahoney MG, DiPersio CM. Reduced fibulin-2 contributes to loss of basement membrane integrity and skin blistering in mice lacking integrin α3β1 in the epidermis. *J Invest Dermatol*. 2014;134(6):1609-1617. doi:10.1038/jid.2014.10
28. Baird BN, Schliekelman MJ, Ahn Y-H, et al. Fibulin-2 is a driver of malignant progression in lung adenocarcinoma. *PLoS One*. 2013;8:e67054.
29. Hulleman JD, Genereux JC, Nguyen A. Mapping wild-type and R345W fibulin-3 intracellular interactomes. *Exp Eye Res*. 2016;153:165-169.
30. Kasetti RB, Maddineni P, Millar JC, Clark AF, Zode GS. Increased synthesis and deposition of extracellular matrix proteins leads to endoplasmic reticulum stress in the trabecular meshwork. *Sci Rep*. 2017;7:14951.
31. Sun Z, Brodsky JL. Protein quality control in the secretory pathway. *J Cell Biol*. 2019;218:3171-3187.
32. Guilliams M, Bonnardel J, Haest B, et al. Spatial proteogenomics reveals distinct and evolutionarily conserved hepatic macrophage niches. *Cell*. 2022;185:379-396.e38.
33. Robert S, Gicquel T, Bodin A, Lagente V, Boichot E. Characterization of the MMP/TIMP imbalance and collagen production induced by IL-1β or TNF-α release from human hepatic stellate cells. *PLoS One*. 2016;11:e0153118.
34. Xu L, Hui AY, Albanis E, et al. Human hepatic stellate cell lines, LX-1 and LX-2: new tools for analysis of hepatic fibrosis. *Gut*. 2005;54:142-151.
35. Tian H, Liu J, Chen J, Gatza ML, Blobe GC. Fibulin-3 is a novel TGF-β pathway inhibitor in the breast cancer microenvironment. *Oncogene*. 2015;34:5635-5647.
36. Xu X, Yang C, Yu X, Wang J. Fibulin-3 regulates the inhibitory effect of TNF-α on chondrocyte differentiation partially via the TGF-β/Smad3 signaling pathway. *Biochim Biophys Acta Mol Cell Res*. 2022;1869:119285.
37. Maniotis AJ, Chen CS, Ingber DE. Demonstration of mechanical connections between integrins, cytoskeletal filaments, and nucleoplasm that stabilize nuclear structure. *Proc Natl Acad Sci USA*. 1997;94:849-854.
38. Wang N, Tytell JD, Ingber DE. Mechanotransduction at a distance: mechanically coupling the extracellular matrix with the nucleus. *Nat Rev Mol Cell Biol*. 2009;10:75-82.
39. Thomas CH, Collier JH, Sfeir CS, Healy KE. Engineering gene expression and protein synthesis by modulation of nuclear shape. *Proc Natl Acad Sci USA*. 2002;99:1972-1977.

40. Burridge K, Guilluy C. Focal adhesions, stress fibers and mechanical tension. *Exp Cell Res*. 2016;343:14-20.
41. Zhao X-K, Yu L, Cheng M-L, et al. Focal adhesion kinase regulates hepatic stellate cell activation and liver fibrosis. *Sci Rep*. 2017;7:4032.
42. Legerstee K, Houtsmuller AB. A layered view on focal adhesions. *Biology (Basel)*. 2021;10:1189.
43. Parsons JT. Focal adhesion kinase: the first ten years. *J Cell Sci*. 2003;116:1409-1416.
44. Zhao X-K, Cheng Y, Liang Cheng M, et al. Focal adhesion kinase regulates fibroblast migration via integrin beta-1 and plays a central role in fibrosis. *Sci Rep*. 2016;6:19276.
45. Huveneers S, Truong H, Fässler R, Sonnenberg A, Danen EHJ. Binding of soluble fibronectin to integrin alpha5 beta1—link to focal adhesion redistribution and contractile shape. *J Cell Sci*. 2008;121:2452-2462.
46. Ilić D, Kovacic B, Johkura K, et al. FAK promotes organization of fibronectin matrix and fibrillar adhesions. *J Cell Sci*. 2004;117:177-187.
47. Naba A. Ten years of extracellular matrix proteomics: accomplishments, challenges, and future perspectives. *Mol Cell Proteomics*. 2023;22:100528.
48. Krasny L, Paul A, Wai P, Howard BA, Natrajan RC, Huang PH. Comparative proteomic assessment of matrisome enrichment methodologies. *Biochem J*. 2016;473:3979-3995.
49. Knittel T, Kobold D, Piscaglia F, et al. Localization of liver myofibroblasts and hepatic stellate cells in normal and diseased rat livers: distinct roles of (myo-)fibroblast subpopulations in hepatic tissue repair. *Histochem Cell Biol*. 1999;112:387-401.
50. Knittel T, Kobold D, Saile B, et al. Rat liver myofibroblasts and hepatic stellate cells: different cell populations of the fibroblast lineage with fibrogenic potential. *Gastroenterology*. 1999;117:1205-1221.
51. Balog S, Fujiwara R, Pan SQ, et al. Emergence of highly profibrotic and proinflammatory Lrat+Fbln2+ HSC subpopulation in alcoholic hepatitis. *Hepatology*. 2023;78:212-224.
52. Sakane S, Hikita H, Shirai K, et al. Proteomic analysis of serum extracellular vesicles reveals Fibulin-3 as a new marker predicting liver-related events in MASLD. *Hepatol Commun*. 2024;8:e0448.
53. Kobayashi N, Kostka G, Garbe JHO, et al. A comparative analysis of the fibulin protein family. Biochemical characterization, binding interactions, and tissue localization. *J Biol Chem*. 2007;282(16):11805-11816. doi:10.1074/jbc.M611029200
54. Dou C-Y, Cao C-J, Wang Z, et al. EFEMP1 inhibits migration of hepatocellular carcinoma by regulating MMP2 and MMP9 via ERK1/2 activity. *Oncol Rep*. 2016;35:3489-3495.
55. Hu J, Duan B, Jiang W, Fu S, Gao H, Lu L. Epidermal growth factor-containing fibulin-like extracellular matrix protein 1 (EFEMP1) suppressed the growth of hepatocellular carcinoma cells by promoting Semaphorin 3B(SEMA3B). *Cancer Med*. 2019;8:3152-3166.
56. Plotnikov SV, Pasapera AM, Sabass B, Waterman CM. Force fluctuations within focal adhesions mediate ECM-rigidity sensing to guide directed cell migration. *Cell*. 2012;151:1513-1527.
57. Woodard DR, Daniel S, Nakahara E, et al. A loss-of-function cysteine mutant in fibulin-3 (EFEMP1) forms aberrant extracellular disulfide-linked homodimers and alters extracellular matrix composition. *Hum Mutat*. 2022;43(12):1945-1955. doi:10.1002/humu.24452
58. Murtha LA, Hardy SA, Mabotuwana NS, et al. Fibulin-3 is necessary to prevent cardiac rupture following myocardial infarction. *Sci Rep*. 2023;13:14995.
59. Tan J, Cai S, Luo X, et al. Stop codon variant in EFEMP1 is associated with primary open-angle glaucoma due to impaired regulation of aqueous humor outflow. *Exp Eye Res*. 2024;241:109859.
60. Livingstone I, Uversky VN, Furniss D, Wiberg A. The pathophysiological significance of fibulin-3. *Biomolecules*. 2020;10:1294.
61. Klenotic PA, Munier FL, Marmorstein LY, Anand-Apte B. Tissue inhibitor of metalloproteinases-3 (TIMP-3) is a binding partner of epithelial growth factor-containing fibulin-like extracellular matrix protein 1 (EFEMP1). Implications for macular degenerations. *J Biol Chem*. 2004;279:30469-30473.
62. Albig AR, Neil JR, Schiemann WP. Fibulins 3 and 5 antagonize tumor angiogenesis in vivo. *Cancer Res*. 2006;66:2621-2629.

SUPPORTING INFORMATION

Additional supporting information can be found online in the Supporting Information section at the end of this article.

How to cite this article: Thomas C, Bouezzedine F, Bonnier D, Legagneux V, Théret N. Proteomic analysis of liver fibrosis reveals EFEMP1 as a new modulator of focal adhesion and migration of hepatic stellate cells. *The FASEB Journal*. 2025;39:e70515. doi:10.1096/fj.202403086RR